Research article

Dynamical plane wave solutions for the Heisenberg model of ferromagnetic spin chains with beta derivative evolution and obliqueness

M.F. Uddin [a], M.G. Hafez [a,*], S.A. Iqbal [a,b]

[a] *Department of Mathematics, Chittagong University of Engineering and Technology, Chattogram-4349, Bangladesh*
[b] *Department of Electrical and Electronic Engineering, International Islamic University Chittagong, Chattogram 4225, Bangladesh*

A R T I C L E   I N F O

A B S T R A C T

The oblique plane waves with their dynamical behaviors for a (2 + 1)-dimensional nonlinear Schrödinger equation (NLSE) having beta derivative spatial-temporal evolution are investigated. In order to study such phenomena, NLSE is converted to a nonlinear ordinary differential equation with a planar dynamical system by considering the variable wave transform with obliqueness and the properties of the beta derivative. Some more new general forms of analytical solutions, like bright, dark, singular, and pure periodic solutions of NLSE are constructed by employing the auxiliary ordinary differential equation method and the extended simplest equation method. The effect of obliqueness and beta derivative parameter on several types of wave structures along with the phase portrait diagrams are reported by considering some special values of parameters for the existence of attained solutions. It is found that the planar dynamical system is not supported by any type of orbit for $\Theta = 45^0$. It is also confirmed from the obtained solutions that no plane waves are generated for $\Theta = 45^0$. The presented studies on bifurcation analysis and analytical solutions for (2+1)-dimensional NLSE would be very useful to understand the physical scenarios of nonlinear spin dynamics in magnetic materials for Heisenberg models of ferromagnetic spin chains.

1. Introduction

The nonlinear dynamics of the Heisenberg models of ferromagnetic spin chains with magnetic interactions having classical and semi-classical limits associated with soliton spin excitations in condensed matter physics have been reported by many researchers [1, 2, 3, 4, 5, 6, 7]. Such phenomena have been studied by deriving a mathematical physics equation from the aforementioned model, namely, nonlinear Schrödinger equation (NLSE). Because mathematical physics equations [8, 9, 10, 11, 12, 13, 14, 15, 16] provide an arena to study the physical issues not only in the aforementioned system but also in other diverse physical systems. The details of the derivation of NLSE from the Heisenberg model are given in Ref. [8]. Besides, the nonlinear spin excitations in magnetic materials have plenteous real-world applications, e.g., microwave communication systems, magnetic and spintronic devices having signal processing along with magnetic field sensors, high-density data storage materials, and so on [4, 5]. In addition, magnetic nano-objects are one kind of magnetic structure that is produced by synthesizing [6, 7]. Such objects contain alternating magnetic ions and radicals with distinct spins of the order of a dozen Bohr magnetons. In such situations, nonlinear effects play an important role in understanding the dynamical features of these objects. Excitingly, nontrivial topological spin-textures exist in the ground state configuration of ferromagnets due to the balance between Heisenberg exchange interactions that may generate two-dimensional chiral modulations. However, researchers have proposed the following governing completely integrable NLSE for describing a (2 + 1)-dimensional bilinear and anisotropic Heisenberg model of a ferromagnetic spin chain due to the semi-classical limit in Ref. [8]:

$$i\phi_t - i\phi_x + \phi_{xx} + \phi_{yy} - 2\phi_{xy} + 2|\phi|^2\phi = 0. \tag{1}$$

Eq. (1) is a very useful classical model equation to describe the magnetic soliton excitation by considering only the conservative system as well as the system with the presence of locality. It is noted that $\phi(x, y, t)$ represents the normalized complex amplitude of the wave profile. Many

---

* Corresponding author.
  E-mail address: hafez@cuet.ac.bd (M.G. Hafez).

Table 1. Nomenclature/Abbreviations.

Nomenclature/Abbreviations	Explanation
NLSE	Nonlinear Schrödinger Equation
FDs	Fractional Derivatives
BD	Beta–Derivative
AODEM	Auxiliary Ordinary Differential Equation Method
ESEM	Extended Simplest Equation Method
ODE	Ordinary Differential Equation
PDS	Planar Dynamical System
BDE	Beta–Derivative Evolution
OPWSs	Oblique Plane Wave Solutions

research scholars [17, 18, 19, 20, 21, 22, 23, 24, 25, 26, 27, 28, 29, 30, 31, 32, 33] have devoted significant effort to revealing various types of traveling wave solutions for mathematical physics equations like Eq. (1) by considering many environments via several types of theoretical and computational architectures. But classical models are not actually useful for divulging the effect of memory [34] due to their time-consuming nature, which is mainly manifest in non-local and non-conservative physical systems. In most real-world problems, it is sometimes not possible to describe the features of physical issues by only the integer-order NLEEs. Because the complexity may arise in a certain regime of either space or time for the impact of non-locality as well as non-conservative energies of materials. From a physical point of view, this will happen only when the scale approaches a very small one. In such situations, only the fractional order NLEEs and their analytical solutions are applicable. To overcome such difficulties, researchers have concentrated their efforts on fractional derivatives (FDs), such as conformable, Caputo, Riemann-Liouville derivatives, etc., in lieu of classical derivatives. Such FDs have been introduced in many mathematical physics equations [20, 31, 32, 34, 35, 36, 37, 38, 39] to understand the complex physical issues in the physical system. Very recently, the newly included FD, so called the Beta derivative (BD), has been proposed by Atangana et al. [37], which fulfills all the fundamental features of calculus and overcomes some limitations of the aforementioned FDs. BD can not only be considered as FD but also be considered as a natural extension of the classical derivative [38]. Further, the most expedient way is to study the plane waves by including direction cosines to the uniform plane waves because they do not generally occur with incidence. One can mainly study the magnetic solitonic excitations by considering only the $(2+1)$-dimensional mathematical physics equations. That is, the wave propagation might be studied by considering it parallel and perpendicular to the magnetic field. Due to the importance of fractional effects and obliqueness, Uddin et al. [20] have already determined the periodic and rouge wave solutions by considering the following $(2+1)$–dimensional NLSE along with beta derivative evolution (BDE) via the generalized exponential expansion method and the modified Kudryashov method:

$$i\left(\begin{smallmatrix}A\\0\end{smallmatrix}D_t^\beta \phi\right) - i\left(\begin{smallmatrix}A\\0\end{smallmatrix}D_x^\beta \phi\right) + \left[\left(\begin{smallmatrix}A\\0\end{smallmatrix}D_{xx}^{2\beta}\right) + \left(\begin{smallmatrix}A\\0\end{smallmatrix}D_{yy}^{2\beta}\right)\right]\phi - 2\left(\begin{smallmatrix}A\\0\end{smallmatrix}D_{xx}^{2\beta}\phi\right) + 2|\phi|^2\phi = 0. \tag{2}$$

They have only focused on the periodic and rogue structures with the influence of BDE and obliqueness without considering the dynamical analysis of planar dynamical systems (PDS). They have also not mentioned whether or not the plane wave exists depending on the obliqueness. But there are numerous possibilities for determining a more general form of oblique plane wave solutions (OPWSs) of Eq. (2) in order to comprehend the nature of other types of coherent structures in the aforementioned system. Because researchers have reported only several types of solutions without considering obliqueness and BDE in the previous literature [17, 18, 19, 21, 22, 23, 24]. Further, Uddin et al. [20] have also highlighted only periodic singular and rogue wave structures by considering the aforementioned equation. The bifurcation features have also not been demonstrated for Eq. (2) in the previous studies to the best of our knowledge. However, one can determine some more new general forms of OPWSs, like bright, dark, pure periodic, and singular solutions to Eq. (2) with the involvement of BDE and obliqueness. Further research into the dynamical behaviors of nonlinear spin dynamics for Heisenberg ferromagnetism with magnetic interactions described by $(2+1)$-dimensional NLSE with BDE under the influence of obliqueness and fractional parameter is therefore required. Also, one needs to determine some more new and general forms of OPWSs of Eq. (2) via suitable solution methods based on the stability conditions.

Thus, this work explores the bifurcation analysis of plane waves by forming PDS from the considered equation. In addition, some more new analytical forms of OPWSs are determined by employing two useful techniques, namely, the auxiliary ordinary differential equation method (AODEM) [32, 39] and the extended simplest equation method (ESEM) [33]. The effect of BD parameter and obliqueness on several types of wave structures, along with the phase portrait diagrams are examined. The detailed study of this paper is organized as follows: In Sec. 2, the corresponding nonlinear ordinary differential equation (ODE) with PDS of the considered NLSE having BDE is derived. In Sec. 3 and Sec. 4, we recapitulate AODEM and ESEM, respectively, in a concise way and they are implemented to explore the OPWSs of the considered NLSE with physical interpretation. Finally, in Sec. 5, the conclusion is drawn.

1.1. Notations

The nomenclature and abbreviations used throughout this study are provided in Table 1.

2. PDS for NLSE having BDE and bifurcation analysis

This section begins with the traveling wave variable transformation to convert Eq. (2) into its equivalent ODE:

$$\phi(x, y, t) = U(\zeta)e^{i\Lambda(x,y,t)}, \tag{3}$$

where

$$\zeta = \frac{\cos\Theta}{\beta}\left(x + \frac{1}{\Gamma\beta}\right)^\beta + \frac{\sin\Theta}{\beta}\left(y + \frac{1}{\Gamma\beta}\right)^\beta + \frac{\alpha}{\beta}\left(t + \frac{1}{\Gamma\beta}\right)^\beta$$

and

$$\Lambda = -\left[\frac{\cos\Theta}{\beta}\left(x + \frac{1}{\Gamma\beta}\right)^\beta + \frac{\sin\Theta}{\beta}\left(y + \frac{1}{\Gamma\beta}\right)^\beta\right] + \frac{\upsilon}{\beta}\left(t + \frac{1}{\Gamma\beta}\right)^\beta$$
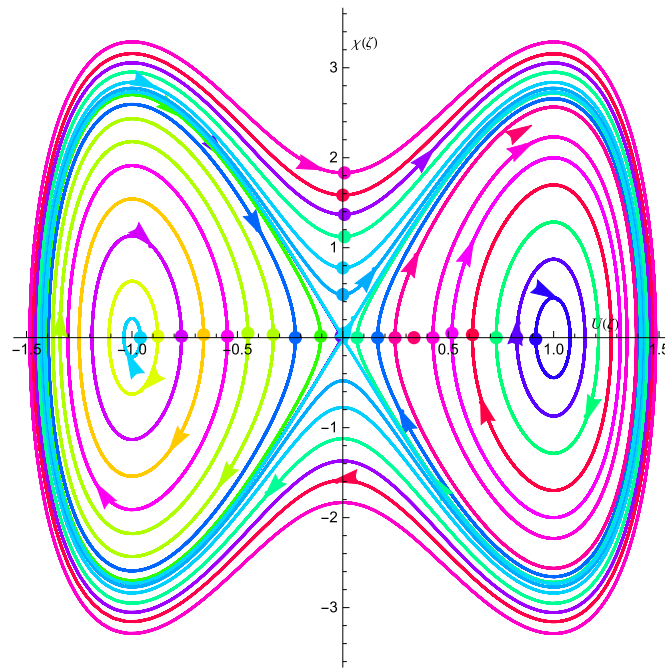
Fig. 1. Phase portrait diagram of Eq. (7) for $v = 1$ and $\Theta = 30^0$.

Here, $U(\zeta)$ represents the shape of the pulse, $\Lambda(x, y, t)$ is the phase component, α and v are the speed and number of waves, respectively. Also, one needs to define BD along with some basic properties for converting ODE. To do so, the BD is defined [37, 38] as

$$
{}_0^A D_\zeta^\beta \, \aleph(\zeta) = \lim_{\epsilon \to 0} \frac{\aleph\left(\zeta + \epsilon\left(\zeta + \frac{1}{\Gamma(\beta)}\right)^{1-\beta}\right) - \aleph(\zeta)}{\epsilon}
\tag{4}
$$

The BD properties are also given as follows:

(i). ${}_0^A D_\zeta^\beta \left\{ \lambda_1 \aleph_1(\zeta) + \lambda_2 \aleph_2(\zeta) \right\} = \lambda_1 \, {}_0^A D_\zeta^\beta \left\{ \aleph_1(\zeta) \right\} + \lambda_2 \, {}_0^A D_\zeta^\beta \left\{ \aleph_2(\zeta) \right\}$; $\lambda_1, \lambda_2 \in \mathfrak{R}$

(ii). ${}_0^A D_\zeta^\beta \left\{ \lambda \right\} = 0$; $\lambda \in \mathfrak{R}$

(iii). ${}_0^A D_\zeta^\beta \left\{ \aleph_1(\zeta) \cdot \aleph_2(\zeta) \right\} = \aleph_1(\zeta) \cdot {}_0^A D_\zeta^\beta \left\{ \aleph_2(\zeta) \right\} + \aleph_2(\zeta) \cdot {}_0^A D_\zeta^\beta \left\{ \aleph_1(\zeta) \right\}$

(iv). ${}_0^A D_\zeta^\beta \left\{ \aleph_1(\zeta) / \aleph_2(\zeta) \right\} = \dfrac{\aleph_2(\zeta) \cdot {}_0^A D_\zeta^\beta \left\{ \aleph_1(\zeta) \right\} - \aleph_1(\zeta) \cdot {}_0^A D_\zeta^\beta \left\{ \aleph_2(\zeta) \right\}}{\aleph_2^2(\zeta)}$.

Here $\aleph_2(\zeta) \neq 0$ and $\aleph_1(\zeta)$ are β-differentiable functions with $\beta \in (0, 1]$. By inserting $\epsilon = \left(\zeta + \frac{1}{\Gamma(\beta)}\right)^{\beta-1} \tau$, when $\epsilon \to 0$, $\tau \to 0$ in Eq. (4), another important property of BD is defined as

$$
{}_0^A D_\zeta^\beta \, \aleph(\zeta) = \left(\zeta + \frac{1}{\Gamma(\beta)}\right)^{1-\beta} \frac{d\aleph(\zeta)}{d\zeta}.
\tag{5}
$$

Eq. (2) is then converted to an ODE by using Eq. (3) along with the BD property as in Eq. (5).

$$
(\cos\Theta - \sin\Theta)^2 U''(\zeta) - \left[(\cos\Theta - \sin\Theta)^2 + \cos\Theta + v \right] U(\zeta) + 2U^3(\zeta) = 0,
\tag{6}
$$

where $\alpha = 2\sin 2\Theta - \cos\Theta - 2$.

Now, Eq. (6) is converted to the next one-dimensional ODE system for investigating the dynamical nature of the model Eq. (2) as

$$
\begin{aligned}
\frac{dU(\zeta)}{d\zeta} &= \chi(\zeta) \\
\frac{d\chi(\zeta)}{d\zeta} &= \frac{S}{(\cos\Theta - \sin\Theta)^2} U(\zeta) - \frac{2}{(\cos\Theta - \sin\Theta)^2} U^3(\zeta),
\end{aligned}
\tag{7}
$$

where $S = (\cos\Theta - \sin\Theta)^2 + \cos\Theta + v$.

The Jacobi matrix for the ODE system as in Eq. (7) is given as

$$
J\left(U_E, \chi_E\right) = \begin{pmatrix} 0 & 1 \\ \frac{S}{(\cos\Theta - \sin\Theta)^2} - \frac{6}{(\cos\Theta - \sin\Theta)^2} U^2(\zeta) & 0 \end{pmatrix}.
\tag{8}
$$

For the state points, that is, $\left(U_E, \chi_E\right) = (0, 0), (\pm\sqrt{S/2}, 0)$, the obtained eigenvalues of the system as in Eq. (7) are presented in Table 2 and Table 3, respectively, based on the Jacobi matrix as in Eq. (8) and the parametric values $v = \pm 1$ and $\Theta = 30^0$:

When $v = 1$ & $\Theta = 30^0$, three state points with their corresponding eigenvalues for Eq. (7) are given as in Table 2. It is clear from Table 2 that the origin indicates an unstable saddle-node, whereas the other two state points represent two stable homoclinic orbits, which are connected from
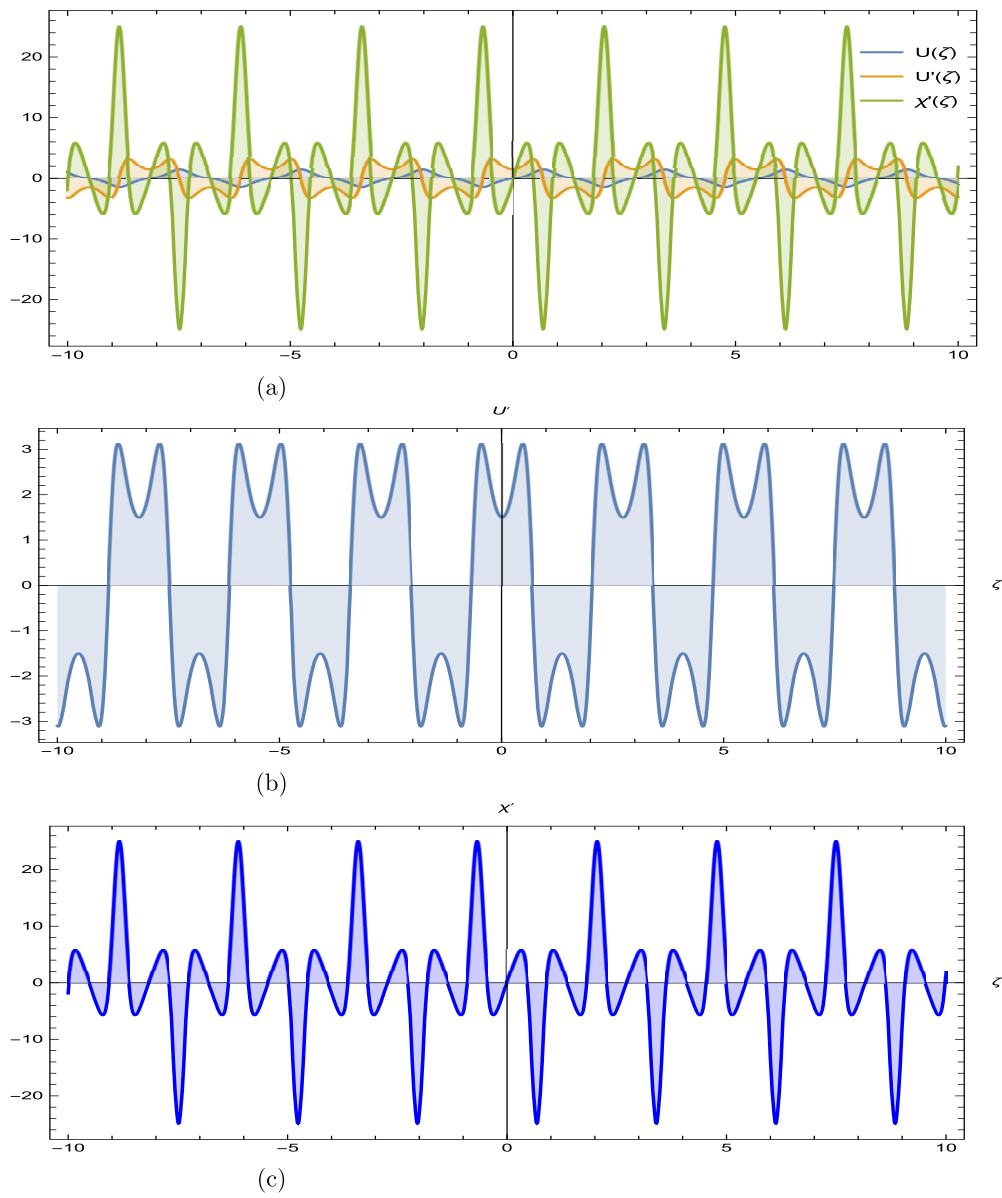
Fig. 2. Diagrams of time scale for (a) U, U', χ' (b) U' with regards to ζ and (c) χ' with regards to ζ of Eq. (7) with $v = 1$ and $\Theta = 30^0$.
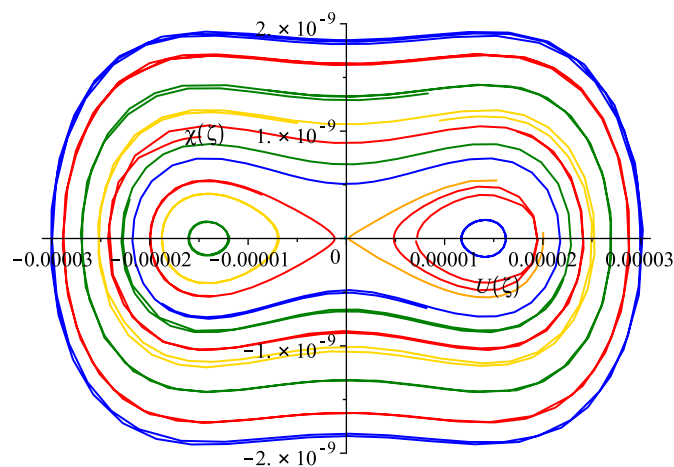

Fig. 3. Phase portrait diagram of Eq. (7) for $v = -1$ and $\Theta = 30^0$.
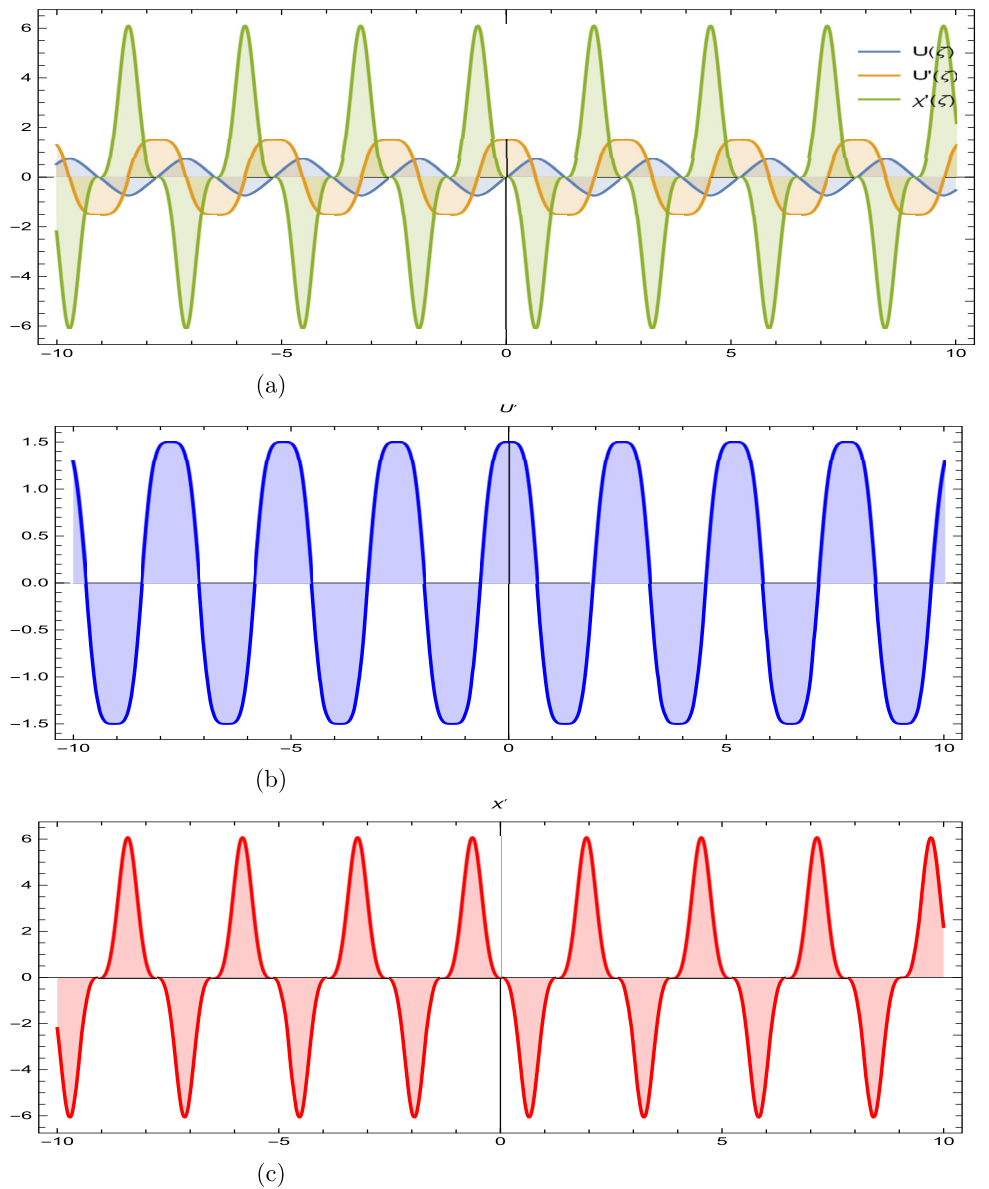
Fig. 4. Diagrams of time scale for (a) U, U', χ' (b) U' with regards to ζ and (c) χ' with regards to ζ of Eq. (7) with $v = -1$ and $\Theta = 30^0$.

Table 2. Phase State Classify for $v = 1$, $\& \, \Theta = 30^0$.

Eigenvalues and State Point Classifications			
State points	$(0,0)$	$(-1,0)$	$(1,0)$
Eigenvalues	± 3.86	$\pm 5.46i$	$\pm 5.46i$
Classifications	*Unstable & Saddle*	*Stable & Center*	*Stable & Center*

Table 3. Phase State Classify for $v = -1$, $\& \, \Theta = 30^0$.

Eigenvalues and State Point Classifications			
State points	$(0,0)$	$(-1.41 \times 10^{-5}, 0)$	$(1.41 \times 10^{-5}, 0)$
Eigenvalues	$\pm 5.46 \times 10^{-5}$	$\pm 7.73 \times 10^{-5} i$	$\pm 5.46i$
Classifications	*Unstable & Saddle*	*Stable & Center*	*Stable & Center*

the left-hand side to the right-hand side. The phase portraits and time scale diagrams for Eq. (7) based on the above values are depicted in Fig. 1 and Fig. 2, respectively. It is clearly observed from Fig. 1 that the saddle-node bifurcations are described by a family of periodic kinks and anti-kink shattering wave solutions for Eq. (2). Besides, the phase portrait diagram and time scale interpretation for Eq. (7) are displayed in Fig. 3 and Fig. 4, respectively, based on the values $v = -1$ and $\Theta = 30^0$. It is clearly observed from Table 3 and Fig. 3 that the equilibrium point is unstable and saddle at the origin. In contrast, the other state points are stable and center. Fig. 3 also indicates that the model Eq. (2) has a solitary and breaking wave solution corresponding to a pair of homoclinic orbits at the state points $(0,0), (\pm 1.41 \times 10^{-5}, 0)$. But a remarkable output of this work is that when $v < 0$ is chosen, all three equilibrium points tend to the center. For example, at $v = -1$, the system has three equilibrium points, which are almost identical to the origin. The phase portrait looks like the same pattern as in Fig. 1 compared to Fig. 3 on a small-scale simulation. But if one simulates
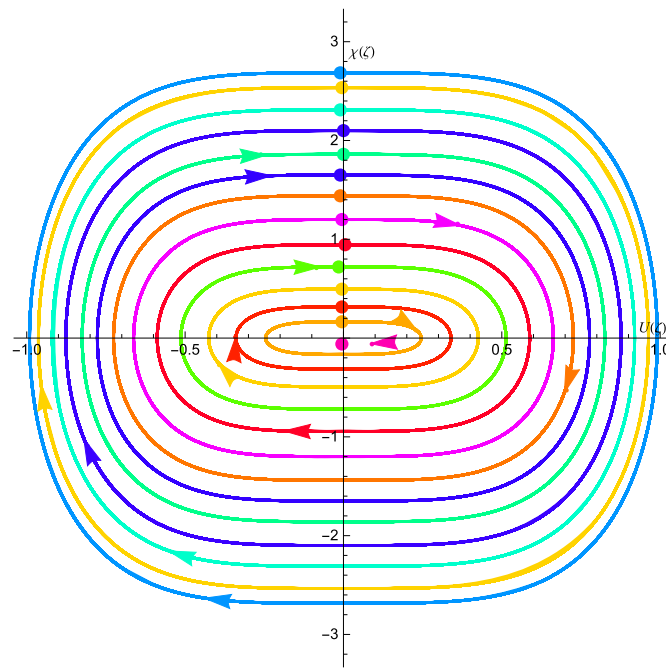
Fig. 5. Phase portrait diagram of Eq. (7) for $v = -2$ and $\Theta = 30^0$.

the phase state on a large scale for the same specified values, then the simulation for soliton orbits will move and center at the stable node $(0,0)$. If v is chosen to be less than -1, then the system has only one real equilibrium point $(0,0)$, and the other two nodes will be imaginary. To illustrate it, Fig. 5 displays the phase diagram of Eq. (7) by considering $v = -2$, which clearly indicates that the real state point is $(0,0)$ and the other phase state might be moving around the origin. In such a situation, Eq. (2) represents only the oscillatory wave solution, except for soliton or shock wave solutions. Based on Figs. 2 and 4, the soliton orbits are predicted. They are not converging, but trajectories are moving around the center nodes. It is noted that the system is valid for $0^0 \leq \Theta \leq 90^0$ and v's real values, except $\Theta = 45^0$. If we chose $\Theta = 45^0$, the model fails to express any dynamical behaviors. Furthermore, no traveling waves are formed because no type of orbit exists for the assumed parametric value of $\Theta = 45^0$.

3. OPWSs via AODEM with parametric investigations

According to the homogeneous balance principle and AODEM (see details in Ref. [39]), the oblique solutions of Eq. (6) can be expressed as a polynomial in $H(\zeta)$:

$$U(\zeta) = \sum_{N=0}^{1} \lambda_N H^N(\zeta), \tag{9}$$

where, $\lambda_N (N = 0, 1)$ are constants with $\lambda_1 \neq 0$. The function $H(\zeta)$ is the exact solution of the following auxiliary ODE:

$$H'(\zeta) = \sqrt{pH^2(\zeta) + qH^4(\zeta) + rH^6(\zeta)}. \tag{10}$$

It is mentioned here that Eq. (10) offers a variety of solutions by applying to the actual parametric values p, q and r as set out in Ref. [39]. With the help of Eq. (9) and Eq. (10), a polynomial in $H(\zeta)$ from Eq. (6) is obtained. By setting the coefficients of this polynomial equal to zero, a set of algebraic equations for $\lambda_0, \lambda_1, p, q, r$ and v are formulated, which are ignored for convenience. By simplifying the resulting equations, one obtains

$$\lambda_0 = 0, \ \lambda_1 = \pm\sqrt{q(\sin 2\Theta - 1)}, \ v = (1-p)(\sin 2\Theta - 1) - \cos\Theta, \ p = p, \ q = q, \ r = 0.$$

Based on the values of the above constants together with the solutions of Eq. (10) and with the assistance of Eqs. (3) and (9), the following exact OPWSs for the considered NLSE including BDE are determined:

Case-I: When $p > 0$,

$$\phi_1(x,y,t) = \pm\exp\left(i\left[-\left\{\frac{\cos\Theta}{\beta}\left(x + \frac{1}{\Gamma(\beta)}\right)^\beta + \frac{\sin\Theta}{\beta}\left(y + \frac{1}{\Gamma(\beta)}\right)^\beta\right\} + \frac{v}{\beta}\left(t + \frac{1}{\Gamma(\beta)}\right)^\beta\right]\right)$$
$$\times \frac{\sqrt{p(1 - \sin 2\Theta)}}{\cosh\left\{\sqrt{p}\left[\frac{\cos\Theta}{\beta}\left(x + \frac{1}{\Gamma(\beta)}\right)^\beta + \frac{\sin\Theta}{\beta}\left(y + \frac{1}{\Gamma(\beta)}\right)^\beta + \frac{\alpha}{\beta}\left(t + \frac{1}{\Gamma(\beta)}\right)^\beta\right]\right\}}, \tag{11}$$

$$\phi_2(x,y,t) = \pm\exp\left(i\left[-\left\{\frac{\cos\Theta}{\beta}\left(x + \frac{1}{\Gamma(\beta)}\right)^\beta + \frac{\sin\Theta}{\beta}\left(y + \frac{1}{\Gamma(\beta)}\right)^\beta\right\} + \frac{v}{\beta}\left(t + \frac{1}{\Gamma(\beta)}\right)^\beta\right]\right)$$
$$\times \frac{\sqrt{p(\sin 2\Theta - 1)}}{\sinh\left\{\sqrt{p}\left[\frac{\cos\Theta}{\beta}\left(x + \frac{1}{\Gamma(\beta)}\right)^\beta + \frac{\sin\Theta}{\beta}\left(y + \frac{1}{\Gamma(\beta)}\right)^\beta + \frac{\alpha}{\beta}\left(t + \frac{1}{\Gamma(\beta)}\right)^\beta\right]\right\}}, \tag{12}$$
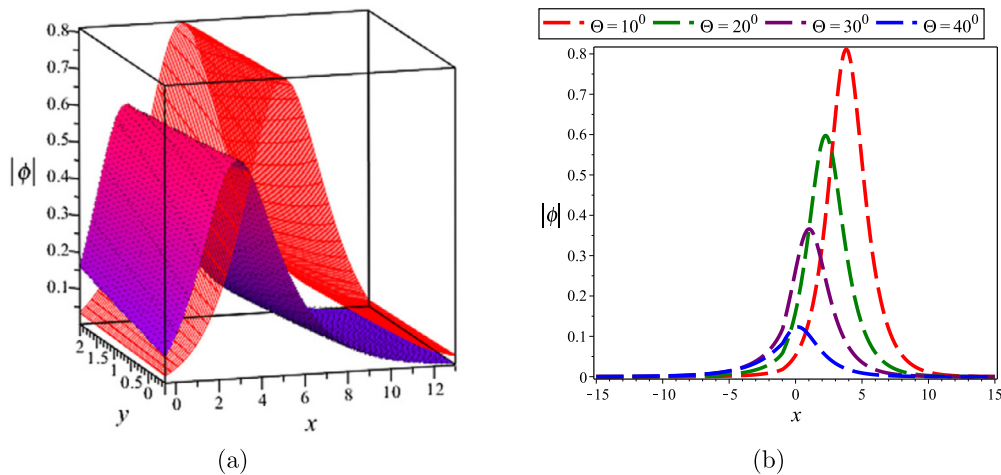
Fig. 6. 3D and 2D shapes of the wave profile of modulus (ϕ) analogous to Eq. (13) for (a) several values of obliqueness $\Theta = 10^0$ (red) and $\Theta = 20^0$ (magenta), (b) effect of Θ for $\beta = 0.9$ along the x-axis, keeping y constant. All the other remaining parameters are considered as $p = 1, q = 1, r = 0$ and $t = 1$.

$$\phi_3(x,y,t) = \pm \exp\left(i\left[-\left\{ \frac{\cos\Theta}{\beta}\left(x + \frac{1}{\Gamma(\beta)}\right)^\beta + \frac{\sin\Theta}{\beta}\left(y + \frac{1}{\Gamma(\beta)}\right)^\beta \right\} + \frac{v}{\beta}\left(t + \frac{1}{\Gamma(\beta)}\right)^\beta \right]\right)$$
$$\times \sqrt{\frac{2p(\sin 2\Theta - 1)}{\cosh\left\{ 2\sqrt{p}\left[\frac{\cos\Theta}{\beta}\left(x + \frac{1}{\Gamma(\beta)}\right)^\beta + \frac{\sin\Theta}{\beta}\left(y + \frac{1}{\Gamma(\beta)}\right)^\beta + \frac{\alpha}{\beta}\left(t + \frac{1}{\Gamma(\beta)}\right)^\beta \right]\right\} - 1}}, \tag{13}$$

$$\phi_4(x,y,t) = \pm \exp\left(i\left[-\left\{ \frac{\cos\Theta}{\beta}\left(x + \frac{1}{\Gamma(\beta)}\right)^\beta + \frac{\sin\Theta}{\beta}\left(y + \frac{1}{\Gamma(\beta)}\right)^\beta \right\} + \frac{v}{\beta}\left(t + \frac{1}{\Gamma(\beta)}\right)^\beta \right]\right)$$
$$\times \sqrt{\frac{2p(\sin 2\Theta - 1)}{i\sinh\left\{ 2\sqrt{p}\left[\frac{\cos\Theta}{\beta}\left(x + \frac{1}{\Gamma(\beta)}\right)^\beta + \frac{\sin\Theta}{\beta}\left(y + \frac{1}{\Gamma(\beta)}\right)^\beta + \frac{\alpha}{\beta}\left(t + \frac{1}{\Gamma(\beta)}\right)^\beta \right]\right\} - 1}}, \tag{14}$$

$$\phi_5(x,y,t) = \pm \exp\left(i\left[-\left\{ \frac{\cos\Theta}{\beta}\left(x + \frac{1}{\Gamma(\beta)}\right)^\beta + \frac{\sin\Theta}{\beta}\left(y + \frac{1}{\Gamma(\beta)}\right)^\beta \right\} + \frac{v}{\beta}\left(t + \frac{1}{\Gamma(\beta)}\right)^\beta \right]\right)$$
$$\times \frac{\sqrt{pq(\sin 2\Theta - 1)}\sqrt{\exp\left(2\sqrt{p}\left[\frac{\cos\Theta}{\beta}\left(x + \frac{1}{\Gamma(\beta)}\right)^\beta + \frac{\sin\Theta}{\beta}\left(y + \frac{1}{\Gamma(\beta)}\right)^\beta + \frac{\alpha}{\beta}\left(t + \frac{1}{\Gamma(\beta)}\right)^\beta \right]\right)}}{\exp\left(2\sqrt{p}\left[\frac{\cos\Theta}{\beta}\left(x + \frac{1}{\Gamma(\beta)}\right)^\beta + \frac{\sin\Theta}{\beta}\left(y + \frac{1}{\Gamma(\beta)}\right)^\beta + \frac{\alpha}{\beta}\left(t + \frac{1}{\Gamma(\beta)}\right)^\beta \right]\right) - 4q}, \tag{15}$$

Case-II: When $p < 0$,

$$\phi_6(x,y,t) = \pm \exp\left(i\left[-\left\{ \frac{\cos\Theta}{\beta}\left(x + \frac{1}{\Gamma(\beta)}\right)^\beta + \frac{\sin\Theta}{\beta}\left(y + \frac{1}{\Gamma(\beta)}\right)^\beta \right\} + \frac{v}{\beta}\left(t + \frac{1}{\Gamma(\beta)}\right)^\beta \right]\right)$$
$$\times \sqrt{\frac{2p(\sin 2\Theta - 1)}{\cos\left\{ 2\sqrt{-p}\left[\frac{\cos\Theta}{\beta}\left(x + \frac{1}{\Gamma(\beta)}\right)^\beta + \frac{\sin\Theta}{\beta}\left(y + \frac{1}{\Gamma(\beta)}\right)^\beta + \frac{\alpha}{\beta}\left(t + \frac{1}{\Gamma(\beta)}\right)^\beta \right]\right\} - 1}}, \tag{16}$$

$$\phi_7(x,y,t) = \pm \exp\left(i\left[-\left\{ \frac{\cos\Theta}{\beta}\left(x + \frac{1}{\Gamma(\beta)}\right)^\beta + \frac{\sin\Theta}{\beta}\left(y + \frac{1}{\Gamma(\beta)}\right)^\beta \right\} + \frac{v}{\beta}\left(t + \frac{1}{\Gamma(\beta)}\right)^\beta \right]\right)$$
$$\times \sqrt{\frac{2p(\sin 2\Theta - 1)}{\sin\left\{ 2\sqrt{-p}\left[\frac{\cos\Theta}{\beta}\left(x + \frac{1}{\Gamma(\beta)}\right)^\beta + \frac{\sin\Theta}{\beta}\left(y + \frac{1}{\Gamma(\beta)}\right)^\beta + \frac{\alpha}{\beta}\left(t + \frac{1}{\Gamma(\beta)}\right)^\beta \right]\right\} - 1}}, \tag{17}$$

where, $\alpha = 2\sin 2\Theta - \cos\Theta - 2$, $v = (1 - p)(\sin 2\Theta - 1) - \cos\Theta$. It is noted that the OPWSs as in Eqs. (11), (12), (13), (14), (15), (16) and (17) are obtained by considering $\varepsilon = 1$ from the solutions of Eq. (10) (see Ref. [39]). Another solution set for $\varepsilon = -1$ from the solutions of Eq. (10) can be easily secured, which is ignored for simplicity. Based on the attained solutions of NLSE having BDE, some of the outcomes are displayed graphically (see Figs. 6–8) to demonstrate the effectiveness of β and Θ. The parametric values are assumed within the ranges of $0 < \beta \le 1$ and $0 < \Theta < \pi/2$ and are based on the conditions of the considered method. These figures explore how the beta fractional parameter and obliqueness are remarkably changed in the plane wave phenomena. Figs. 6a and 6b demonstrate that the amplitudes and widths of traveling waves decrease with the increasing value of Θ. It is provided that the plane waves lose their energy with the increase in obliqueness. Besides, Figs. 7a and 7b show that the amplitudes are almost the same but the widths of the waves are decreased due to the increase of the β parameter, and pulse-like hump-shaped rightward wave
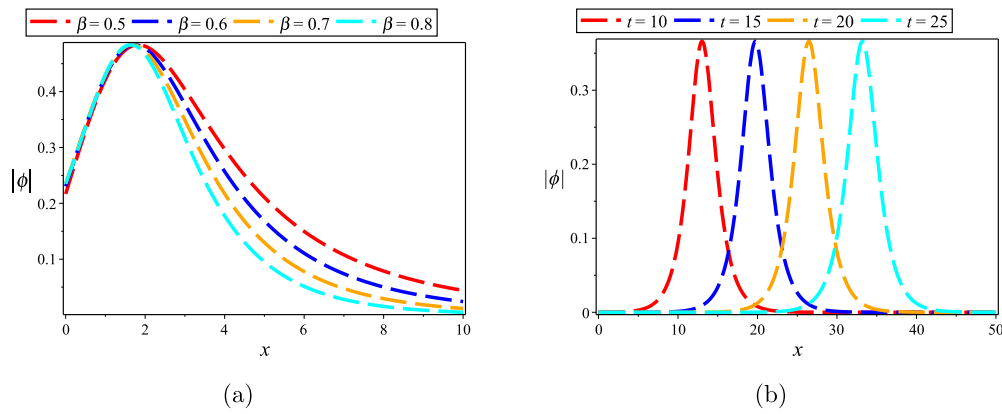
(a)

(b)

Fig. 7. 2D shape of wave profile of modulus (ϕ) analogous to Eq. (13) for (a) several values of β with $\Theta = 25^0$ and (b) several values of t with $\Theta = 30^0$, $\beta = 0.9$ along the x-axis, keeping y constant. All the other remaining parameters are considered as in Fig. 6.
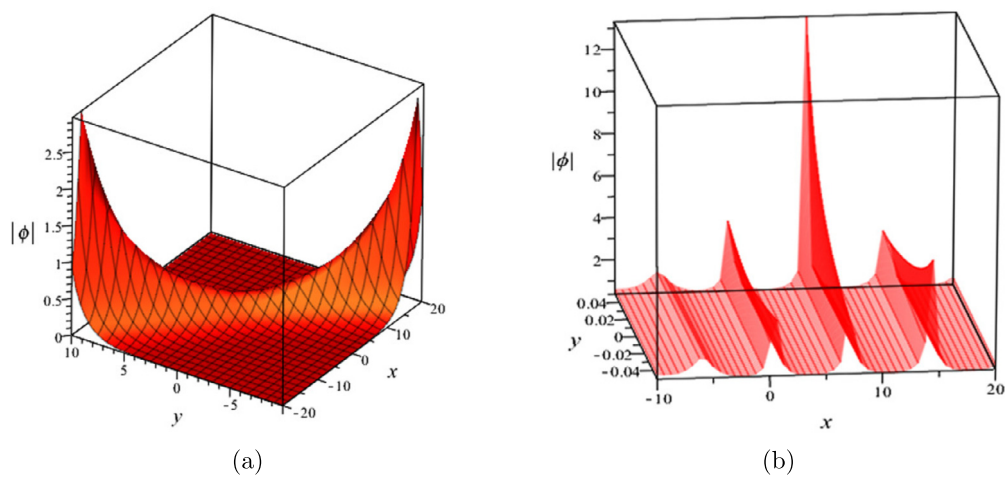

(a)

(b)

Fig. 8. 3D shape of wave profile of modulus of ϕ as revealed in (a) Eq. (15) for $p = 1$, $q = -1$ and (b) Eq. (17) for $p = -1$, $q = 1$ with $\beta = 0.95$, $\Theta = 60^0$ respectively. Other parameters are considered as $r = 0$, $t = 1$.

structures are found with the increase of time. In addition, Figs. 8a and 8b exhibit the singular soliton and periodic traveling wave type shapes of the modulus of ϕ by considering the parametric values based on the stability condition. It is also found that the AODEM provided some more new general forms of OPWSs for NLSE having BDE that were not determined in the previous literature [20].

4. OPWSs via ESEM with parametric investigations

Starting this section with a brief description of ESEM to extract analytic solutions of the considered NLSE. Let us consider the projective Riccati equation [33] as follows:

$$\psi'(\zeta) = -\psi(\zeta)\,\chi(\zeta), \quad \chi'(\zeta) = -\chi^2(\zeta) + \sigma\psi(\zeta) - \mu, \tag{18}$$

where, σ and μ are constants. Assume the solutions of Eq. (18) as

$$\psi(\zeta) = \frac{1}{H(\zeta)}, \quad \chi(\zeta) = \frac{H'(\zeta)}{H(\zeta)}. \tag{19}$$

Using Eq. (19), the function $H(\zeta)$ satisfies the following equivalent converted second-order linear ODE for Eq. (18):

$$H''(\zeta) + \mu H(\zeta) = \sigma. \tag{20}$$

Now, one can easily obtain three types of general solutions to Eq. (20) as follows:

Case-I: For $\mu < 0$,

$$H(\zeta) = C_1 \cosh\left(\sqrt{-\mu}\,\zeta\right) + C_2 \sinh\left(\sqrt{-\mu}\,\zeta\right) + \frac{\sigma}{\mu}, \tag{21}$$

so that

$$\left(\frac{H'(\zeta)}{H(\zeta)}\right)^2 = \varpi_1 \left(\frac{1}{H(\zeta)}\right)^2 - \mu + \frac{2\sigma}{H(\zeta)}; \quad where, \quad \varpi_1 = \mu\left(C_1^2 - C_2^2\right) - \frac{\sigma^2}{\mu}. \tag{22}$$

Case-II: For $\mu > 0$,

$$H(\zeta) = C_1 \cos\left(\sqrt{\mu}\,\zeta\right) + C_2 \sin\left(\sqrt{\mu}\,\zeta\right) + \frac{\sigma}{\mu}, \tag{23}$$

so that

$$\left(\frac{H'(\zeta)}{H(\zeta)}\right)^2 = \varpi_2 \left(\frac{1}{H(\zeta)}\right)^2 - \mu + \frac{2\sigma}{H(\zeta)}; \; where, \; \varpi_2 = \mu\left(C_1^2 + C_2^2\right) - \frac{\sigma^2}{\mu}, \tag{24}$$

Case-III: For $\mu = 0$,

$$H(\zeta) = \frac{\sigma}{2}\zeta^2 + C_1\zeta + C_2, \tag{25}$$

so that

$$\left(\frac{H'(\zeta)}{H(\zeta)}\right)^2 = \varpi_3 \left(\frac{1}{H(\zeta)}\right)^2 + \frac{2\sigma}{H(\zeta)}; \; where, \; \varpi_3 = C_1^2 - 2\sigma C_2. \tag{26}$$

In all the above cases, C_1 and C_2 are considered arbitrary constants. Now, according to the ESEM, the OPWSs of Eq. (6) can be expressed as a finite power series in the form:

$$U(\zeta) = \sum_{r=0}^{N} \lambda_r \left(\frac{H'(\zeta)}{H(\zeta)}\right)^r + \sum_{s=0}^{N-1} \gamma_s \left(\frac{H'(\zeta)}{H(\zeta)}\right)^s \left(\frac{1}{H(\zeta)}\right), \tag{27}$$

where $N = 1$ is determined from Eq. (6) by using the homogeneous balancing principal and λ_r $(r = 0, 1)$, and γ_s $(s = 0)$ are constants to be determined later with $\lambda_N^2 + \gamma_{N-1}^2 \neq 0$. The function $H(\zeta)$ is the exact solution of the second-order linear ODE Eq. (20). Now, by substituting Eq. (27) together with the second-order linear ODE (20) and the relationships as in Eqs. (22), (24) and (26) in Eq. (6), one can derive three new polynomials, respectively, in different powers of $\frac{1}{(H(\zeta))^m}$, and $\frac{H'(\zeta)}{(H(\zeta))^n}$ $(m = 0, 1, 2, 3; \; n = 1, 2, 3)$. Setting each coefficient of these polynomials to zero, one can attain a set of algebraic equations for $\lambda_0, \lambda_1, \gamma_0, \sigma, \mu$ and v, which are ignored for simplicity. After simplifying the resulting equations through the computational package Maple, one obtains the following three types of results:

Result-1 (For Case-I): When $\mu < 0$,

$$\lambda_0 = 0 \qquad\qquad \lambda_1 = \pm\frac{1}{2}\sqrt{2\sin\Theta\cos\Theta - 1}$$

$$\gamma_0 = \pm\frac{1}{2}\sqrt{(2\sin\Theta\cos\Theta - 1)\,\varpi_1} \qquad v = \frac{1}{2}(2-\mu)(2\sin\Theta\cos\Theta - 1) - \cos\Theta$$

Based on these constants together with Eq. (21), the OPWS of the considered Eq. (2) is achieved by combining Eqs. (3) and (27) as

$$\phi_8(x, y, t) = \pm\sqrt{-\mu\Delta}\,\exp\left(i\left[-\left\{\frac{\cos\Theta}{\beta}\left(x + \frac{1}{\Gamma(\beta)}\right)^\beta + \frac{\sin\Theta}{\beta}\left(y + \frac{1}{\Gamma(\beta)}\right)^\beta\right\} + \frac{v}{\beta}\left(t + \frac{1}{\Gamma(\beta)}\right)^\beta\right]\right)$$

$$\times \frac{\left\{\sqrt{\frac{\varpi_1}{-\mu}} + C_1\sinh\left(\sqrt{-\mu}\left[\frac{\cos\Theta}{\beta}\left(x + \frac{1}{\Gamma(\beta)}\right)^\beta + \frac{\sin\Theta}{\beta}\left(y + \frac{1}{\Gamma(\beta)}\right)^\beta + \frac{\alpha}{\beta}\left(t + \frac{1}{\Gamma(\beta)}\right)^\beta\right]\right) + C_2\cosh\left(\sqrt{-\mu}\left[\frac{\cos\Theta}{\beta}\left(x + \frac{1}{\Gamma(\beta)}\right)^\beta + \frac{\sin\Theta}{\beta}\left(y + \frac{1}{\Gamma(\beta)}\right)^\beta + \frac{\alpha}{\beta}\left(t + \frac{1}{\Gamma(\beta)}\right)^\beta\right]\right)\right\}}{2\left\{\frac{\sigma}{\mu} + C_1\cosh\left(\sqrt{-\mu}\left[\frac{\cos\Theta}{\beta}\left(x + \frac{1}{\Gamma(\beta)}\right)^\beta + \frac{\sin\Theta}{\beta}\left(y + \frac{1}{\Gamma(\beta)}\right)^\beta + \frac{\alpha}{\beta}\left(t + \frac{1}{\Gamma(\beta)}\right)^\beta\right]\right) + C_2\sinh\left(\sqrt{-\mu}\left[\frac{\cos\Theta}{\beta}\left(x + \frac{1}{\Gamma(\beta)}\right)^\beta + \frac{\sin\Theta}{\beta}\left(y + \frac{1}{\Gamma(\beta)}\right)^\beta + \frac{\alpha}{\beta}\left(t + \frac{1}{\Gamma(\beta)}\right)^\beta\right]\right)\right\}}, \tag{28}$$

where, $\Delta = 2\sin\Theta\cos\Theta - 1$.

Result-2 (For Case-II): When $\mu > 0$,

$$\lambda_0 = 0 \qquad\qquad \lambda_1 = \pm\frac{1}{2}\sqrt{2\sin\Theta\cos\Theta - 1}$$

$$\gamma_0 = \pm\frac{1}{2}\sqrt{(2\sin\Theta\cos\Theta - 1)\,\varpi_2} \qquad v = \frac{1}{2}(2-\mu)(2\sin\Theta\cos\Theta - 1) - \cos\Theta$$

Through the Eqs. (3), (23) and (27), the exact OPWS of Eq. (2) is achieved as

(a)   (b)
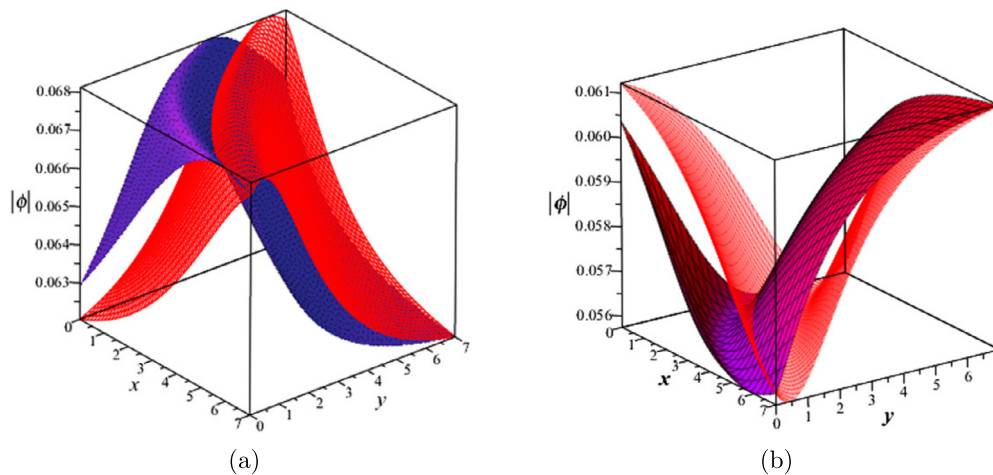
Fig. 9. 3D shape of wave profile of $|\phi|$ as displayed in Eq. (28) for different values of non-local operator parameter (a) $\beta = 0.5$ (blue color surface) and $\beta = 0.7$ (red color surface) with $\sigma = 0.2$ and (b) $\beta = 0.5$ (blue-magenta color surface) and $\beta = 0.7$ (red color surface) with $\sigma = -0.2$. The other parameters are considered as $C_1 = 2$, $C_2 = 0$, $\mu = -1$, $\Theta = 50^0$, and $t = 10$.

$$\phi_9(x,y,t) = \pm\sqrt{\mu\Delta}\ \exp\left(i\left[-\left\{\frac{\cos\Theta}{\beta}\left(x+\frac{1}{\Gamma(\beta)}\right)^\beta + \frac{\sin\Theta}{\beta}\left(y+\frac{1}{\Gamma(\beta)}\right)^\beta\right\} + \frac{v}{\beta}\left(t+\frac{1}{\Gamma(\beta)}\right)^\beta\right]\right)$$

$$\times\frac{\left\{\begin{array}{l}\sqrt{\dfrac{\varpi_2}{\mu}} - C_1\sin\left(\sqrt{\mu}\left[\dfrac{\cos\Theta}{\beta}\left(x+\dfrac{1}{\Gamma(\beta)}\right)^\beta + \dfrac{\sin\Theta}{\beta}\left(y+\dfrac{1}{\Gamma(\beta)}\right)^\beta + \dfrac{\alpha}{\beta}\left(t+\dfrac{1}{\Gamma(\beta)}\right)^\beta\right]\right)\\[4mm] + C_2\cos\left(\sqrt{\mu}\left[\dfrac{\cos\Theta}{\beta}\left(x+\dfrac{1}{\Gamma(\beta)}\right)^\beta + \dfrac{\sin\Theta}{\beta}\left(y+\dfrac{1}{\Gamma(\beta)}\right)^\beta + \dfrac{\alpha}{\beta}\left(t+\dfrac{1}{\Gamma(\beta)}\right)^\beta\right]\right)\end{array}\right\}}{2\left\{\begin{array}{l}\dfrac{\sigma}{\mu} + C_1\cos\left(\sqrt{\mu}\left[\dfrac{\cos\Theta}{\beta}\left(x+\dfrac{1}{\Gamma(\beta)}\right)^\beta + \dfrac{\sin\Theta}{\beta}\left(y+\dfrac{1}{\Gamma(\beta)}\right)^\beta + \dfrac{\alpha}{\beta}\left(t+\dfrac{1}{\Gamma(\beta)}\right)^\beta\right]\right)\\[4mm] + C_2\sin\left(\sqrt{\mu}\left[\dfrac{\cos\Theta}{\beta}\left(x+\dfrac{1}{\Gamma(\beta)}\right)^\beta + \dfrac{\sin\Theta}{\beta}\left(y+\dfrac{1}{\Gamma(\beta)}\right)^\beta + \dfrac{\alpha}{\beta}\left(t+\dfrac{1}{\Gamma(\beta)}\right)^\beta\right]\right)\end{array}\right\}},\tag{29}$$

where, $\Delta = 2\sin\Theta\cos\Theta - 1$.

Result-3 (For Case-III): When $\mu = 0$,

$$\lambda_0 = 0 \qquad\qquad \lambda_1 = \pm\frac{1}{2}\sqrt{2\sin\Theta\cos\Theta - 1}$$

$$\gamma_0 = \pm\frac{1}{2}\sqrt{(2\sin\Theta\cos\Theta - 1)\varpi_3} \qquad v = 2\sin\Theta\cos\Theta - \cos\Theta - 1$$

With the assistance of Eqs. (3), (25) and (27), the OPWS of Eq. (2) is achieved as

$$\phi_{10}(x,y,t) = \pm\sqrt{\Delta}\ \exp\left(i\left[-\left\{\frac{\cos\Theta}{\beta}\left(x+\frac{1}{\Gamma(\beta)}\right)^\beta + \frac{\sin\Theta}{\beta}\left(y+\frac{1}{\Gamma(\beta)}\right)^\beta\right\} + \frac{v}{\beta}\left(t+\frac{1}{\Gamma(\beta)}\right)^\beta\right]\right)$$

$$\times\frac{\left\{\sigma\left[\dfrac{\cos\Theta}{\beta}\left(x+\dfrac{1}{\Gamma(\beta)}\right)^\beta + \dfrac{\sin\Theta}{\beta}\left(y+\dfrac{1}{\Gamma(\beta)}\right)^\beta + \dfrac{\alpha}{\beta}\left(t+\dfrac{1}{\Gamma(\beta)}\right)^\beta\right] + C_1 + \sqrt{\varpi_3}\right\}}{\left\{\begin{array}{l}\left\{\sigma\left[\dfrac{\cos\Theta}{\beta}\left(x+\dfrac{1}{\Gamma(\beta)}\right)^\beta + \dfrac{\sin\Theta}{\beta}\left(y+\dfrac{1}{\Gamma(\beta)}\right)^\beta + \dfrac{\alpha}{\beta}\left(t+\dfrac{1}{\Gamma(\beta)}\right)^\beta\right]\right\}^2\\[4mm] + 2\left[\dfrac{\cos\Theta}{\beta}\left(x+\dfrac{1}{\Gamma(\beta)}\right)^\beta + \dfrac{\sin\Theta}{\beta}\left(y+\dfrac{1}{\Gamma(\beta)}\right)^\beta + \dfrac{\alpha}{\beta}\left(t+\dfrac{1}{\Gamma(\beta)}\right)^\beta\right]C_1 + 2C_2\end{array}\right\}},\tag{30}$$

where, $\Delta = 2\sin\Theta\cos\Theta - 1$. It is mentioned here that one can also classify different types of wave structures from the obtained analytical solutions as in Eqs. (28), (29), and (30) based on the values of considered parameters and arbitrary constants used in the ESEM. Based on **Result-1**, one can obtain bright (dark) solitary wave structures by setting $C_1 \neq 0$, $C_2 = 0$, $\sigma > 0(\sigma < 0)$ and $\varpi_1 < 0$, whereas the singular wave structures are constructed by setting $C_1 = 0$, $C_2 \neq 0$, any value of σ and $\varpi_1 > 0$. It is also investigated that periodic wave solutions are obtained when $\varpi_2 < 0$, and either $C_1 \neq 0$, $C_2 = 0$ or $C_2 \neq 0$, $C_1 = 0$. There exists a periodic singularity only for the settings of $\varpi_2 > 0$ with any arbitrary choices of C_1, and C_2 from **Result-2**. It is observed that the OPWSs as in Eqs. (28) and (29) obtained by ESEM are equivalent to the solutions as in Eqs. (14) and (16) in Ref. [20] obtained by the generalized exponential expansion method if $C_2 = 0$. Otherwise, the ESEM provides some more general forms of OPWSs for the considered NLSE. Additionally, a few results are presented graphically (see Figs. 9–13) to illustrate the effectiveness of this extended method with the non-local derivative operator and obliqueness, along with the relevant physical discussions.

Figs. 9a and 9b visualize the 3D shapes of the bright and dark solitary wave profiles of $|\phi|$, respectively, for different non-local values of the BD operator β, whereas the impact for local and non-local values of parameter (β), obliqueness (Θ), and time (t) are illustrated in Figs. 10a - 10d,
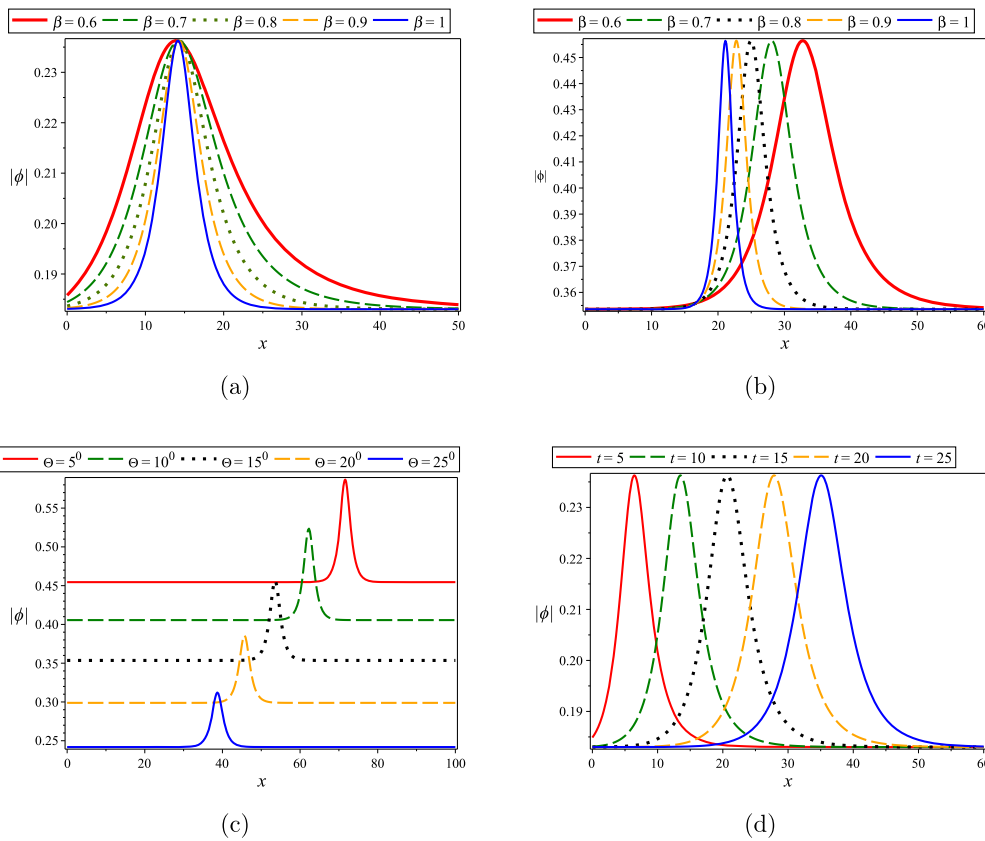
Fig. 10. 2D shape of wave profile of $|\phi|$ as displayed in Eq. (28) for several values of (a) non-local operator β for $\Theta = 60^0$ and (b) $\Theta = 15^0$ with $t = 10$, (c) obliqueness Θ for $\beta = 0.95$, $t = 25$ and (d) t for $\beta = 0.7$, $\Theta = 30^0$ respectively. The remaining parameters are considered as in Fig. 9.
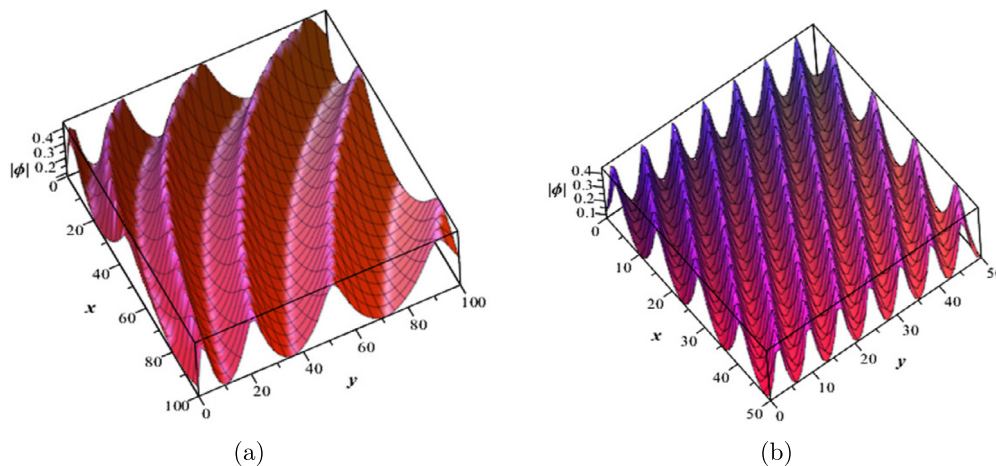

Fig. 11. 3D shape of wave profile of $|\phi|$ as revealed in Eq. (29) for the case of (a) non-local value of $\beta = 0.6$ and (b) local value of $\beta = 1$. The other remaining parameters are considered as $C_1 = -1$, $C_2 = 1$, $\mu = 1$, $\sigma = -2$, $\Theta = 60^0$, and $t = 0.5$.

respectively, based on the solution as in Eq. (28). It is investigated from Figs. 10a and 10b that the beta parameter does not change the size of amplitude but compresses the hump-shaped solitons due to increasing values of β with $\Theta = 60^0$ and $\Theta = 15^0$ respectively. Moreover, the largest amplitude is produced and the solitons propagate from right to left for small values of Θ, while the compressed solitons do not change their position for large Θ. It is also observed that the amplitudes of the pulse-like solitons are decreasing due to an increase in obliqueness, whereas keeping the amplitudes unchanged, only the pulse-widths are increasing over time, which is shown in Figs. 10c and 10d, respectively. Figs. 11a-11b and 12a-12c represent 3D and 2D periodic wave structures along with the effectiveness of parameters β, Θ, and t corresponding to Eq. (29) by considering different constant values of the other parameters. It is observed that the wavelength (frequency) is sufficiently decreased (high) due to increased values of the non-local parameter β. With the increasing values of obliqueness, the amplitudes and wavelengths of the periodic wave structures are decreasing. Additionally, the contour plots are displayed in Figs. 13a and 13b for better visualization of the space-time variation of the wave structures for different values of the β parameter. It is predicted from the above investigations that the non-local derivative operator (β) and obliqueness (Θ) strongly modify the wave structures by using this method for the considered NLSE.
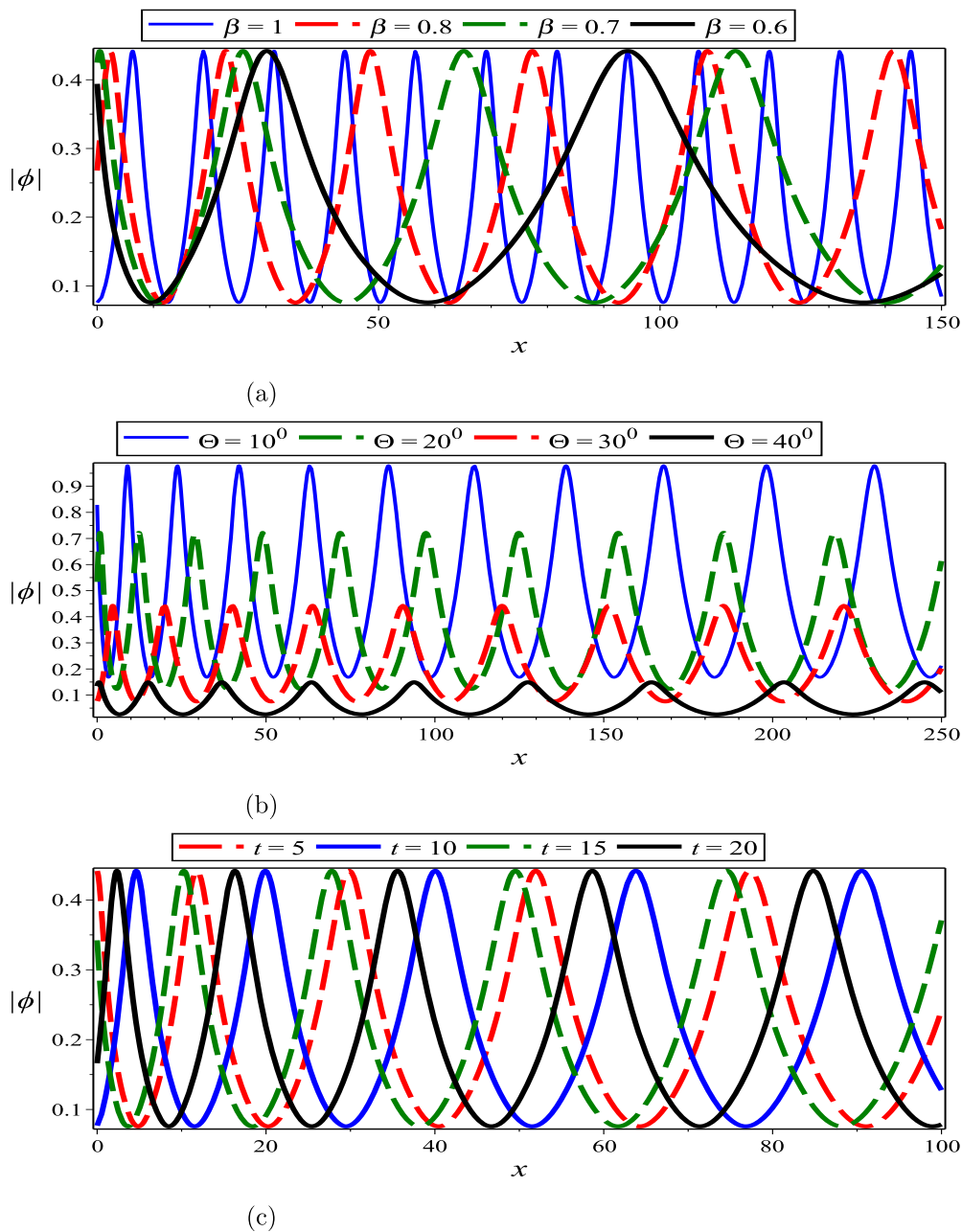
Fig. 12. 2D shape of wave profile of $|\phi|$ as displayed in Eq. (29) for illustrating the effect of (a) non-local operator parameter β for $\Theta = 60^0$, (b) obliqueness Θ for $\beta = 0.7$ with $t = 10$, and (c) time t for $\beta = 0.7$ with $\Theta = 30^0$ respectively. The remaining parameters are considered as in Fig. 11.

5. Concluding remarks

A $(2+1)$-dimensional NLSE having BDE has been considered for reporting the dynamical behaviors and new nonlinear coherent structures arising in many environments, especially in condensed matter physics, optical theories, optical bullets etc., where local/non-local and conservative/non-conservative physical systems are involved. Numerous types of new general forms of OPWSs for such equations have been determined by employing two useful distinct integration schemes, namely, AODEM and ESEM. It is found that the obtained solutions are only dependent on the additional free parameters like p, q, μ and the physical parameters β and Θ. As a result, one can determine various types of useful solutions to understand the nature of wave structures from the proposed solutions based only on the constraint conditions for the additional free parameters. Such conditions have been included in the solutions obtained. In the presented analysis, some of the obtained solutions have been displayed graphically by considering the constraint conditions for the additional parameters. Additionally, the NLSE has been converted to PDS for examining the behavior of bifurcation properties on the basis of the parameters involved. It is observed that the beta fractional parameter (β) and the obliqueness (Θ) significantly change the nature of not only magnetic soliton but also periodic wave propagation, whereas only obliqueness strongly controls the dynamical behavior of plane wave phenomena. It is also being investigated that any types of orbits from PDS are not generated when $\Theta = 45^0$. As a result, no OPWSs are produced as expected based on dynamical analysis. Based on the stability condition, some new structures are demonstrated graphically. Thus, the outcomes presented in this work would be very useful to understand the dynamical features of their wave propagation not only in related fields,
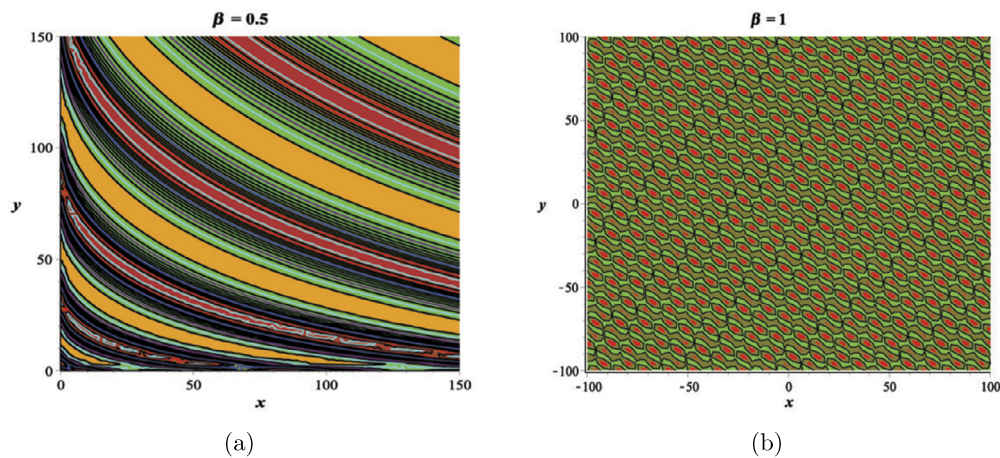
Fig. 13. Contour plot of $|\phi|$ as revealed in Eq. (29) for the (a) non-local value of $\beta = 0.5$ and (b) local value of $\beta = 1$. The remaining parameters are considered as in Fig. 11 except $t = 10$.

especially in microwave communication systems, magnetic and spintronic devices, high-density data storage materials, nano-objects, etc., but also in further laboratory verification.

Declarations

Author contribution statement

M.F. Uddin, M.G. Hafez, S.A. Iqbal: Conceived and designed the analysis; Analyzed and interpreted the data; Contributed analysis tools or data; Wrote the paper.

Funding statement

This research did not receive any specific grant from funding agencies in the public, commercial, or not-for-profit sectors.

Data availability statement

No data was used for the research described in the article.

Declaration of interests statement

The authors declare no conflict of interest.

Additional information

No additional information is available for this paper.

References

[1] M. Lakshmanan, Continuum spin system as an exactly solvable dynamical system, Phys. Lett. A 61 (1977) 53.
[2] G. Huang, Z.P. Shi, X. Dai, R. Tao, Soliton excitations in the alternating ferromagnetic Heisenberg chain, Phys. Rev. B 43 (1991) 11197.
[3] M. Daniel, L. Kavitha, R. Amuda, Soliton spin excitations in an anisotropic Heisenberg ferromagnet with octupole-dipole interaction, Phys. Rev. B 59 (1999) 13774.
[4] P.E. Wigen, Nonlinear Phenomena and Chaos in Magnetic Materials, World Sci, Singapore, 1994.
[5] A.N. Slavin, I.V. Rojdestvenski, Bright and dark spin wave envelope solitons in magnetic films, IEEE Trans. Magn. 30 (1994) 37.
[6] D. Gatteschi, R. Sessoli, J. Villain, Molecular Nano-Magnets, Oxford University Press, New York, 2006.
[7] K. Koumpouras, et al., A spin dynamics approach to solitonics, Sci. Rep. 6 (2016) 25685.
[8] M.M. Latha, C.C. Vasanthi, An integrable model of (2+1)-dimensional Heisenberg ferromagnetic spin chain and soliton excitations, Phys. Scr. 89 (2014) 065204.
[9] A.R. Seadawy, Stability analysis solutions for nonlinear three-dimensional modified Korteweg—de Vries Zakharov—Kuznetsov equation in a magnetized electron—positron plasma, Physica A 455 (2016) 44–51.
[10] A.R. Seadawy, Travelling wave solutions of a weakly nonlinear two-dimensional higher order Kadomtsev-Petviashvili dynamical equation for dispersive shallow water waves, Eur. Phys. J. Plus 132 (2017) 1–13.
[11] L.M. Song, Z.J. Yang, S.M. Zhang, X.L. Li, Spiraling anomalous vortex beam arrays in strongly nonlocal nonlinear media, Phys. Rev. A 99 (2019) 063817.
[12] Z.J. Yang, S.M. Zhang, X.L. Li, Z.G. Pang, Variable sinh-Gaussian solitons in nonlocal nonlinear Schrödinger equation, Appl. Math. Lett. 82 (2018) 64–70.
[13] X. Zhang, J. Jiang, Y. Wu, Y. Cui, Existence and asymptotic properties of solutions for a nonlinear Schrödinger elliptic equation from geophysical fluid flows, Appl. Math. Lett. 90 (2019) 229–237.
[14] A.R. Seadawy, Nonlinear wave solutions of the three-dimensional Zakharov—Kuznetsov—Burgers equation in dusty plasma, Physica A 439 (2015) 124–131.
[15] A.R. Seadawy, Stability analysis for two-dimensional ion-acoustic waves in quantum plasmas, Phys. Plasmas 21 (2014) 052107.
[16] M.G. Hafez, Nonlinear ion acoustic solitary waves with dynamical behaviours in the relativistic plasmas, Astrophys. Space Sci. 365 (2020) 78.
[17] B.Q. Li, Y.L. Ma, Lax pair, Darboux transformation and Nth-order rogue wave solutions for a (2+1)-dimensional Heisenberg ferromagnetic spin chain equation, Comput. Math. Appl. 77 (2019) 514–524.

[18] T.A. Sulaiman, T. Akturk, H. Bulut, H.M. Baskonus, Investigation of various soliton solutions to the Heisenberg ferromagnetic spin chain equation, J. Electromagn. Waves Appl. 32 (2018) 1093–1105.

[19] H. Triki, A.M. Wazwaz, New solitons and periodic wave solutions for the (2+1)-dimensional Heisenberg ferromagnetic spin chain equation, J. Electromagn. Waves Appl. 30 (2016) 788–794.

[20] M.F. Uddin, M.G. Hafez, Z. Hammouch, D. Baleanu, Periodic and rogue waves for Heisenberg models of ferromagnetic spin chains with fractional beta derivative evolution and obliqueness, Waves Random Complex Media 31 (2021) 2135–2149.

[21] D.Y. Liu, B. Tian, Y. Jiang, X.Y. Xie, X.Y. Wu, Analytic study on a (2+1)-dimensional nonlinear Schrödinger equation in the Heisenberg ferromagnetism, Comput. Math. Appl. 71 (2016) 2001–2007.

[22] H. Bulut, T.A. Sulaiman, H.M. Baskonus, Dark, bright and other soliton solutions to the Heisenberg ferromagnetic spin chain equation, Superlattices Microstruct. 123 (2018) 12–19.

[23] M.S. Hashemi, Some new exact solutions of (2+1)-dimensional nonlinear Heisenberg ferromagnetic spin chain with the conformable time fractional derivative, Opt. Quantum Electron. 50 (2018) 79.

[24] M. Inc, A.I. Aliyu, A. Yusuf, D. Baleanu, Optical solitons and modulation instability analysis of an integrable model of (2+1)-dimensional Heisenberg ferromagnetic spin chain equation, Superlattices Microstruct. 112 (2017) 628–638.

[25] M.G. Hafez, Nonlinear Schamel Korteweg-de Vries-Burgers equation to report ion acoustic waves in the relativistic plasmas, IEEE Trans. Plasma Sci. 47 (2019) 5314–5323.

[26] M.G. Hafez, S. Singh, R. Saktivel, S.F. Ahmed, Dust ion acoustic multi-shock wave excitations in the weakly relativistic plasmas with nonthermal nonextensive electrons and positrons, AIP Adv. 10 (2020) 065234.

[27] M.G. Hafez, Face to face collisions of ion acoustic multi-solitons and phase shifts in dense plasma, Braz. J. Phys. 49 (2019) 221.

[28] M.G. Hafez, S.A. Iqbal, S. Akther, M.F. Uddin, Oblique plane waves with bifurcation behaviors and chaotic motion for resonant nonlinear Schrödinger equations having fractional temporal evolution, Results Phys. 15 (2019) 102778.

[29] M.G. Hafez, M.R. Talukder, M.H. Ali, Nonlinear propagation of ion acoustic waves through the Burgers equation in weakly relativistic plasmas, Plasma Phys. Rep. 43 (2017) 499–509.

[30] M.G. Hafez, M.R. Talukder, R. Sakthivel, Ion acoustic solitary waves in plasmas with nonextensive distributed electrons, positrons and relativistic thermal ions, Indian J. Phys. 90 (2016) 603–611.

[31] M.F. Uddin, M.G. Hafez, Z. Hammouch, H. Rezazadeh, D. Baleanu, Traveling wave with beta derivative spatial-temporal evolution for describing the nonlinear directional couplers with metamaterials via two distinct methods, Alex. Eng. J. 60 (2021) 1055–1065.

[32] M.F. Uddin, M.G. Hafez, Interaction of complex short wave envelope and real long wave described by the coupled Schrödinger—Boussinesq equation with variable coefficients and beta space fractional evolution, Results Phys. 19 (2020) 103268.

[33] A.R. Seadawy, H.M. Ahmed, W.B. Rabie, A. Biswas, Chirp-free optical solitons in fiber Bragg gratings with dispersive reflectivity having polynomial law of nonlinearity, Optik 225 (2021) 165681.

[34] J. Singh, D. Kumar, M. Al–Qurashi, D. Baleanu, A new fractional model for giving up smoking dynamics, Adv. Differ. Equ. 2017 (2017) 88.

[35] R. Khalil, M. Al–Horani, A. Yousef, M. Sababheh, A new definition of fractional derivative, J. Comput. Appl. Math. 264 (2014) 65–70.

[36] M. Caputo, M. Fabricio, A new definition of fractional derivative without singular kernel, Prog. Fract. Differ. Appl. 1 (2015) 73–85.

[37] A. Atangana, D. Baleanu, A. Alsaedi, Analysis of time-fractional Hunter-Saxton equation: a model of neumatic liquid crystal, Open Phys. 14 (2016) 145–149.

[38] A. Atangana, D. Baleanu, New fractional derivatives with nonlocal and non-singular kernel: theory and application to heat transfer model, Therm. Sci. 20 (2016) 763–769.

[39] S. Akhter, M.G. Hafez, H. Rezazadeh, Resonance nonlinear wave phenomena with obliqueness and fractional time evolution via the novel auxiliary ordinary differential equation method, SN Appl. Sci. 1 (2019) 567.